D. Burak, W. Nasalski

EXCITATION OF OPTICAL SOLITONS BY HIGHER-ORDER HERMITE-GAUSSIANS

12/1995

WARSZAWA 1995

ISSN 0208-5658

Praca wpłynęła do Redakcji dnia 8 lutego 1995 r.

Na prawach rękopisu

Instytut Podstawowych Problemów Techniki PAN
Nakład 100 egz. Ark. wyd. 1,75 Ark. druk. 2,0
Oddano do drukarni w marcu 1995 r.

Wydawnictwo Spółdzielcze sp. z o.o.
Warszawa, ul. Jasna 1

EXCITATION OF OPTICAL SOLITONS BY HIGHER–ORDER HERMITE–GAUSSIANS

D. Burak and W. Nasalski

Institute of Fundamental Technological Research, Polish Academy of Science, Swietokrzyska 21, 00–049 Warsaw, Poland

Abstract

For the first time, a close link between the higher order optical solitons and the higher order Hermite–Gaussian beams or pulses is shown. The nonlinear propagation of the first– and the second–order optical solitons in a Kerr medium is studied by use of the inverse scattering, numerical and variational approaches. The variational analysis is performed using the first– and the second–order Hermite-Gaussians known from the theory of linear propagation. It is shown that the first– and second–order Hermite Gaussians excite higher–order solitons only of *even* order. A very good agreement is found between variational approximation and direct numerical integration of the nonlinear Schrödinger equation for a wide range of incident beam amplitudes.

I. INTRODUCTION

Since the early theoretical and numerical work on propagation of optical solitons in Kerr medium [1–3], much progress has been made to reveal basic features and indicate applications of these self–maintaining solutions to the nonlinear Schrödinger equation (NSE). The first experimental observation of soliton pulses in optical fibers [4], followed by the demonstration of the dispersionless long distance soliton propagation [5], opened possibilities for the realization of ultrahigh–speed optical transmission systems [6]. It is well known that there is a complete analogy between the temporal solitons, in which nonlinear phase modulation balances dispersion, and spatial solitons, in which self–focusing balances diffraction [1]. A two–dimensional spatial solitons were experimentally observed in planar slab wave guides [7,8] or in bulk materials [9] and semiconductors [10], and their potential implementation in optical switching and signal processing was clearly shown [11,12].

In above mentioned studies the higher–order ($N > 1$) spatial or temporal solitons, besides the fundamental ($N = 1$) solution to NSE, have been, to a some extend, also discussed and their excitation was experimentally confirmed [4,7,9,10]. The higher-order solitons are frequently regarded as the outcome of the interaction between fundamental solitons and described by a set of coupled NSE equations [13,14]. A generalization of the reduced variational approach [15,16] is leading to the straightforward results directly interpreted in terms of the potential well description of the nonlinear process [14]. To be strict, however, the higher–order soliton should be treated as a *single* independent solution to NSE as it appears within a frame of the Inverse Scattering Transform [1,3,17] (IST). That immediately leads to the problem of finding the adequate model of the higher–order soliton excitation and, as well, an appropriate generalization of the reduced variational approach, which could satisfactorily follow the higher–order soliton propagation process.

The paper addresses the question of the close link between the higher–order soliton solutions and higher–order Hermite–Gaussian (HG) beams or pulses. The reduced variational analysis proves that this link is really close on the fundamental solution level; the Gaus-

sian function, as an approximate model of the exact solution, reveals all main features of the fundamental soliton propagation [15]. On the other hand, it has been recently shown [18] that the *nonlinear propagation* of the Gaussian beam or pulse can be *exactly tied to the linear propagation* of the Gaussian beam or pulse with appropriately scaled Gaussian parameters. The simple scaling transformation makes it possible to trace the fundamental soliton propagation by a linear evolution of the Gaussian beam or pulse in the scaled space. The tracing process is governed by the linear scaled complex ray equation jointly fulfilled by all the HG beams or pulses of arbitrary order and that indicates their special role in modeling the excitation and propagation of higher–order optical solitons [18]. Moreover, the phase differences between the side lobes of the first– and the second–order HG simulate the cases of the repelling (for the first–order HG) or attracting (for the second-order HG) pairs of the fundamental solitons. It seems, therefore, that the HG functions could be good candidates for the trial functions in the variational analysis of the higher order nonlinear propagation. This work is, to our knowledge and besides our previous preliminary report [19], the first attempt to verify this conjecture.

The role of the HG beams in the paraxial theory of the linear propagation is well established [20]. Among all the possible solutions to NSE in a low power limit

$$i\frac{\partial U^{(n)}}{\partial \zeta} + \frac{1}{2}\frac{\partial^2 U^{(n)}}{\partial x^2} = 0 \,, \tag{1}$$

where x and ζ are the transverse and the propagation coordinate, respectively, we choose the HG function in a symmetric form proposed by Siegman [21]

$$U^{(n)}(x,\zeta) = A^{(n)}(\zeta)\, v^{-n}(\zeta)\, H_n(y)\, U^{(0)}(x,\zeta) \,, \tag{2}$$

with a complex argument

$$y = 2^{-1/2}\frac{x}{v(\zeta)} \,. \tag{3}$$

They have a normalized form of the fundamental Gaussian beam [22]

$$U^{(0)}(x,\zeta) = v^{-1}(\zeta)\exp(-y^2) \,, \tag{4}$$

multiplied by the Hermite polynomial

$$H_n(y) = (-1)^n \exp(y^2) \frac{d^n}{dy^n} \exp(-y^2) . \tag{5}$$

In Eqs. (2)–(4) $A^{(n)}$ denotes the beam on-axis amplitude at the waist ($\zeta = 0$), the complex beam half-width v

$$v^{-2}(\zeta) = w^{-2}(\zeta) - i\mathcal{R}^{-1}(\zeta) , \tag{6}$$

is expressed by the real half-width w normalized by its initial value w_0, and by the radius of the phase front curvature R normalized by the diffraction length $z_F = k_0 w_0^2$, k_0 being the wave number in the low power limit [22]. In the linear limit $v^2(\zeta)$ linearly depends on ζ: $v^2(\zeta) = 1 + i\zeta$. Only the first three Hermite polynomials are used in the paper as given by

$$H_0(y) = 1 , \; H_1(y) = 2y , \; H_2(y) = -2(1 - 2y^2) . \tag{7}$$

Besides the simplicity of such HG functions, the facts that they serve as natural expansion functions of the electromagnetic field at the linear plane boundary [23] or nonlinear interface [22], and describe the beam field outside the paraxial region [24] promote them as potentially useful trial functions in our analysis.

Our starting point in the variational modelling of the higher–order solitons is the formulation of Anderson [15] for the fundamental soliton propagation. We follow Anderson results (in our compact notation) for the fundamental soliton case and generalize the variational approach to the higher–order soliton cases. However, in our considerations we should assume the general form of the initial conditions for the nonlinear beam or pulse evolution, i.e. non planar phase–front of the beam at the initial plane. That leads to the following potential well equation for the beam half–width w [25]

$$\frac{1}{2} \frac{dw}{d\zeta} = w_0^4 \mathcal{R}_0^{-2} - V(w) , \tag{8}$$

where $V(w)$ is the potential "at rest" for the plane phase front incidence [15] and $\mathcal{R}_0$ is the actual phase front curvature at the initial plane. Therefore, the threshold for the fundamental soliton excitation is given in this general case by

$$A^{(0)} = 2^{-1/4} w_0^{-1} \sqrt{1 + w_0^4 \mathcal{R}_0^{-2}} \,, \tag{9}$$

i. e., it depends not only on the beam width but also on the initial beam convergence magnitude $|\mathcal{R}_0|$ [25]. (note that, in opposite to Eq. (6), the initial value w_0 of w is not assumed in Eqs. (8)–(9) to be equal to one). This fact was also confirmed by the IST analysis [26].

In Section II the IST results are shown for the excitation of the solitons of the first and second order. The variational analysis of their propagation was performed in Section III, and compared with numerical integration results in Section IV. Our results are valid in both cases of optical beams and optical pulses as the two-dimensional (1+1) solutions to NSE. For the compactness of the paper, however, only the beam solutions will be referred to in the text.

II. EXCITATION OF SOLITON PAIRS

In the nonlinear Kerr medium the slowly varying approximation leads to the common form of the nonlinear Schrödinger equation for the electric field envelope

$$i\frac{\partial U}{\partial \zeta} + \frac{1}{2}\frac{\partial^2 U}{\partial x^2} + |U|^2 U = 0 \,. \tag{10}$$

The arbitrary number of eigensolutions (solitons) of NSE (10) was obtained first by Zakharov and Shabat [1]. The general form of single soliton solution

$$U(x,\zeta) = 2\eta e^{2i(\eta^2-\xi^2)\zeta - 2i\xi x} \mathrm{sech}[2\eta x + 4\eta\xi\zeta] \,, \tag{11}$$

corresponds to the beam with amplitude and width 2η, propagating with an angle $\vartheta = -\arctan(2\xi)$ to the ζ–direction. Exact analytic solutions exist for waveforms consisting of multiple solitons with distinct soliton parameters η_i and ξ_i. When they are well separated, each soliton takes the form of solution (11). If N solitons (with amplitudes $2\eta_i$, $i = 1, 2, ...N$) propagate along the ζ–direction (i. e. $\xi_i = 0$, $i = 1, 2, ...N$) they form a bound solution (an example of symmetric centered at $x = 0$ two–soliton solution, called breather soliton, is

given in Ref. [27]). Explicit analytical form of solution of NSE describing collision of two solitons (i. e. propagation of pair of fundamental solitons) was found in Ref. [17]

We study NSE with the initial condition given by the first–order (HG1)

$$U_0^{(1)}(x) = A_0^{(1)}\ H_1\Big(\frac{x}{\sqrt{2}}\Big)\exp\Big(-\frac{x^2}{2}\Big)\,, \tag{12}$$

and second–order (HG2)

$$U_0^{(2)}(x) = A_0^{(2)}\ H_2\Big(\frac{x}{\sqrt{2}}\Big)\ \exp\Big(-\frac{x^2}{2}\Big)\,, \tag{13}$$

Hermite–Gaussian beam entering the Kerr medium in its waist ($\zeta = 0$). In Eqs. (12) and (13) $A_0^{(n)}$ ($n = 1, 2$) stands for the incident beam amplitude.

The parameters of solitons excited by an initial profile $U_0^{(n)}(x)$ are determined by the Zakharov–Shabat scattering equations [1,3] and numerical method solving this eigenvalue problem is presented in Appendix A. Results of our calculations are presented in Fig. 1, where the imaginary and real parts of λ_i are shown (on the left–hand side and right–hand side axes, respectively), as a function of the incident (HG1 or HG2) beam amplitude $A_0^{(n)}$. The process of soliton excitation is schematically presented in Table I. For low incident beam amplitudes no solitons are found [rows labeled as *(A)* in Tab. I]. However, there exists the certain threshold amplitude $A_0^{(thr)}$ (different for each incident beam – see Table I for numerical values), above which the incident (HG1 or HG2) profile splits into *two* solitons which propagate apart with equal amplitudes [rows *(B)* in Tab. I]. In Figs. 2(a) and 3(a) we ilustrate this process for incident HG1 and HG2 beam, respectively . Further increase of the amplitude $A_0^{(n)}$ causes the decrease of relative angle between soliton beams (dotted lines) and the increase of amplitudes of excited solitons (solid lines) [cf. Figs. 1(a) and 1(b)]. In the far field the solution of NSE is in this case given by the sum of two solitons described by Eq. (11).

There is a substantial difference between the excitation of the solitons by antisymmetric (HG1) and symmetric (HG2) initial profiles. In the later case there exists the certain amplitude value $A_0^{(b)}$ for which both eigenvalues collapse, i. e. $\xi_1 = 0 = \xi_2$ and $\eta_1 = \eta_2$. In this

case the incident HG2 beam breaks up into two solitons which propagate in parallel with each other, separated in space [29], as it is shown in Fig 3(b). Further increase of $A_0^{(n)}$ [in the range shown in row *(C)* in Tab. I], for an initial HG2 profile, causes decrease in one value of the soliton amplitude and increase in the value of the another one. Thus the exact two–soliton solution has a form of symmetric breather soliton [27] and an example of such type of solution is presented in Fig. 3(c).

One observes, that the bound soliton solution *cannot* be formed from an *antisymmetric* initial profile given by Eq. (12), as it was first pointed out in Ref. [3]. It is interesting that the numerical results concerning soliton excitation by (real and *symmetric*) HG2 profile [see Fig. 1(b)] seem to contradict the finding of Satsuma and Yajima [3]. According to Theorem III, for the initial condition which is real and not antisymmetric, the eigenvalues λ_i are purely imaginary, i. e. $\xi_i = 0$. This fact follows from the equation [Eq. (27) in Ref. [3]]

$$\xi_i \int_{-\infty}^{+\infty} \left(\varphi_2\varphi_1^* - \varphi_1\varphi_2^*\right)(x,\lambda_i)\mathrm{d}x = i\int_{-\infty}^{+\infty} Im[U_0^{(n)}(x)]\left(|\varphi_1|^2 - |\varphi_2|^2\right)(x,\lambda_i)\mathrm{d}x\ , \qquad (14)$$

where $\varphi_{1,2}(x,\lambda_i)$ are the eigensolutions of Eqs. (A1), and $Im[U_0^{(n)}(x)]$ denotes the imaginary part of the initial profile [Eq. (12) or (13)]: $Im[U_0^{(n)}(x)] = 0$. Since the right–hand side of Eq. (14) has to be zero, Satsuma and Yajima conjectured that $\xi_i = 0$. However, numerical evaluation of the the left–hand side showed, that the integral itself is equal to zero (within the numerical accuracy) for values of the incident beam amplitudes in the range between $A_0^{(thr)}$ and $A_0^{(b)}$, thus allowing $\xi_i \neq 0$. For an antisymmetric and real initial profile HG1 this integral is always equal to zero, as it follows from the symmetry of eigensolutions φ_1 and φ_2 [3], and in this case ξ_i can take non–zero values. Thus, for HG1 beams the propagation directions of the fundamental soliton parts have to be different for finite ζ, meanwhile for HG2 beams the directions can be different or equal, depending on the incident amplitude. This explains the qualitative difference between Figs. 1(a) and 1(b).

With further increase of the incident (HG1 or HG2) beam amplitude $A_0^{(n)}$ [rows labeled as *(D)* in Tab. I] the process of soliton excitation repeats: a new pair of solitons occurs in the

far field. Figures 2(b) and 2(c) show the excitation of zero–amplitude and finite–amplitude second soliton pair, respectively, from the icident HG1 beam. The qualitative dependence of their parameters on the incident (HG1 or HG2) beams amplitude $A_0^{(n)}$ is similar to the behavior discussed above.

III. VARIATIONAL MODELING OF THE NONLINEAR PROPAGATION

In this Section we consider an analytical approximation to nonlinear propagation of first– and second–order Hermite–Gaussian beams using the variational approach developed by Anderson [15]. The Lagrangian associated with Eq. (10) has the form

$$L^{(n)} = \frac{i}{2}\Big[U^{(n)*}\frac{\partial U^{(n)}}{\partial \zeta} - U^{(n)}\frac{\partial U^{(n)*}}{\partial \zeta}\Big] - \frac{1}{2}\Big|\frac{\partial U^{(n)}}{\partial x}\Big|^2 + \frac{1}{2}|U^{(n)}|^4 . \tag{15}$$

Since the nonlinear Schrödinger equation (10) is valid only for small nonlinearities, it is not unreasonable to expect that in some cases the exact solution of NSE can be approximated by the low power solution, i. e. the solution to the linear propagation. Thus we use the following functional form of trial wave function [see Eq. (2)]

$$U^{(1)}(x,\zeta) = \sqrt{2}\; A^{(1)}(\zeta)\; v^{-3}(\zeta)\; x\; \exp\Big(-\frac{x^2}{2v^2(\zeta)}\Big) , \tag{16}$$

in the case of HG1 initial conditions [Eq. (12)], and

$$U^{(2)}(x,\zeta) = 2\; A^{(2)}(\zeta)\; v^{-3}(\zeta)\; \Big[-1 + \Big(\frac{x}{v(\zeta)}\Big)^2\Big]\; \exp\Big(-\frac{x^2}{2v^2(\zeta)}\Big) , \tag{17}$$

for HG2 initial conditions [Eq. (13)], with $A^{(n)}(0) = A_0^{(n)}$ and $v(0) = 1$ [for sake of simplicity of notation we left the superscript (n) in function $v(\zeta)$].

Substituting the trial function ansatz (16) or (17) one can integrate the Lagrangian density (15) over the transverse variable x. Such a reduced Lagrangian is subsequently used in standard Euler–Lagrange equations for beam parameters: $A^{(n)}(\zeta)$ and $v(\zeta)$ [15]. Then, after the straightforward algebra, the ordinary differential equations (ODE model) are obtained in the general form

$$\frac{\mathrm{d}v(\zeta)}{\mathrm{d}\zeta} = P^{(n)}\Big(A^{(n)}(\zeta), v(\zeta)\Big)\,, \tag{18a}$$

$$\frac{\mathrm{d}A^{(n)}(\zeta)}{\mathrm{d}\zeta} = Q^{(n)}\Big(A^{(n)}(\zeta), v(\zeta)\Big)\,. \tag{18b}$$

The analytic expressions of the reduced Lagrangians, complex functions $P^{(n)}$ and $Q^{(n)}$, as obtained for trial functions (16) and (17), are listed in Table II. For completeness of our analysis, the results concerning the fundamental Gaussian beam (HG0) propagation are given in Tab. II. Note, that the constant of integration of the Euler–Lagrange equations: $\int_{-\infty}^{\infty} |U^{(n)}(x,\zeta)|^2 dx$, has the form

$$\frac{|A^{(n)}|^2}{(v^2+v^{*2})^{n+1/2}} = const = \frac{A_0^{(n)2}}{2^{n+1/2}}\,, \tag{19}$$

where n denotes the order of Hermite–Gaussian function. This integration constant is related to the lowest order conserved quantity that the NSE obey [1].

The same structure of functions $P^{(n)}$ and $Q^{(n)}$ (except some multiplication factors) obtained from variational approximation to the HG0 and HG1 beam propagation can be explained as follows. An antisymmetric initial profile (12) induces the gradient of the nonlinear index of refraction which is lowest at the center point between the side lobes (i. e. at $x = 0$). This causes that each part of the incident HG1 beam moves away from the center point and behaves, more or less, as a single HG0 beam, what is reflected in the form of dynamical Eqs. (18). According to this observation one can show that the variational approach to higher–order HG beam propagation exhibits the evidence of the incident threshold beam amplitude $A_0^{(thr)}$ for the fundamental soliton excitation. As it has been mentioned in Introduction, the fundamental, zero–amplitude soliton can be excited from the HG0 beam with the finite radius of the phase front curvature $\mathcal{R}[A_0^{(thr)}]$, if its peak amplitude $A^{(0)}[A_0^{(thr)}]$ and width $w_0[A_0^{(thr)}]$ are related by Eq. (9). The notation used here emhasizes that each value of the side lobe's parameters (i. e. $A^{(0)}$, w_0 and R) depends on the amplitude $A_0^{(n)}$ of the incident beam (in square brakets). Assuming, that each of the side lobes of higher–order HG beam [Eq. (16) or (17)] possesses the HG0 form, one can find numerically [by solving

the ODE model Eqs. (18)] its values of $A^{(0)}[A_0]$, $w_0[A_0]$ and $\mathcal{R}[A_0]$ at different planes of ζ. It is then possible to estimate (using the polynomial extrapolation) what values would take these quantities at infinity: $\zeta = \infty$ (where the soliton with zero amplitude and infinite width should be observed as it is the case for soliton generation threshold). The incident threshold beam amplitude $A_0^{(thr)}$ for the fundamental, zero–amplitude soliton excitation is defined as the amplitude, for which the condition given by Eq. (9) is satisfied. In Fig. 4(a) and 4(b) we show the ratio $\sqrt[4]{2}|U(x_{max},\zeta|w_0$ vs the propagation distance ζ for variational approximation to HG1 and HG2 beam propagation, respectively, where $U(x_{max},\zeta)$ denotes the peak–amplitude of the side lobe and is equal to $A^{(0)}[A_0]$ in Eq. (9). Since the phase–front of each side lobe tends to be a plane, the quantity $\mathcal{R}[A_0]$ tends to infinity and thus the last term on the right–hand–side of Eq. (9) become negligible for a sufficiently large ζ. The threshold incident amplitude for the zero–amplitude soliton excitation is therefore defined as such value of $A_0^{(n)}$ for which the ratio $\sqrt[4]{2}|U(x_{max},\zeta|w_0$ is equal to unity at infinity: $\zeta = \infty$, as it is the case for the smallest incident amplitudes displayed in Fig. 4. Numerical results of our calculations for HG1 and HG2 beams are presented in rows labeled as *(A)* in Table I. The discrepancy in numerical values between variational estimation of $A_0^{(thr)}$ and their actual values, as obtained from IST, follows from assumption that each of the side lobes of HG beam is of the simple Gaussian form with parabolic phase front.

The value of amplitude $A_0^{(b)}$ for bound solution formation from the incident beam (see previous Section) can be determined by investigation of the Hamiltonian function of the system governed by NSE [1]

$$\mathcal{H}^{(n)} = (1/2)\int_{-\infty}^{+\infty}\left(\left|\frac{\partial U^{(n)}}{\partial x}\right|^2 - |U^{(n)}|^4\right)\mathrm{d}x\ . \tag{20}$$

Particular forms of $\mathcal{H}^{(n)}$ for Hermite–Gaussian beams considered in this paper are given in Table II. Numerical solution of ODE model (18) confirms, that the Hamiltonian (20) is conserved in variational approximation to the nonlinear beam propagation. Moreover, it can be inferred from numerical examination of the $\mathcal{H}^{(n)}$ values, that for $\mathcal{H}^{(n)} < 0$ the beam parameters undergo periodic oscillations, for $\mathcal{H}^{(n)} > 0$ beam's complex width $v(\zeta)$

increases to infinity (i. e. the beam undergoes diffraction), and the $\mathcal{H}^{(n)} = 0$ gives the threshold between these two behaviors [13]. Substituting initial conditions for the ODE model $[A^{(n)}(0) = A_0^{(n)}, v(0) = 1]$ into Hamiltonian $\mathcal{H}^{(n)}$ (see Tab. II) the threshold values $A_0^{(b)}$ are found for bound solution (i. e. breather soliton) excitation within the variational approach to HG beams propagation (see Tab. I for numerical values). We point out that in the case of initial HG2 profile (13) this approach leads to a very accurate approximation of the threshold amplitude for formation of the breather soliton $A_0^{(b)}$ (see previous Section), whereas in the case of HG1 beam propagation this prediction is an artifact of the variational method.

The analysis of the ODE model Eqs. (18) enables us to find "Gaussian soliton" solution [15] of the higher-order. This is the case when the parameters of the trial function [i. e. complex width $v(\zeta)$ and amplitude $A^{(n)}(\zeta)$] remain constant as the beam propagates in nonlinear medium. Since the behavior of the system is determined by the first of Eqs. (18) [see Tab. II], the incident beam's amplitude $A_0^{(gs)}$ for excitation of higher-order "Gaussian soliton" solution is determined by the condition: $P^{(n)}(A^{(n)}(0), v(0)) = 0$. Direct calculations show, that the relationship between amplitudes $q^{(gs)}$ and $q^{(b)}$ can be written as: $q^{(gs)} = \sqrt{2}q^{(b)}$, which is the same as for the case of fundamental "Gaussian soliton" excitation [15]. Numerical evaluation of these quantities leads to the value $A_0^{(gs)} = 2\sqrt[4]{2} \approx 2.37$ for HG1 beam, $[A_0^{(gs)} = 4\sqrt{5\sqrt{2}/51} \approx 1.49$ for HG2 beam], and so the amplitude $A_0^{(gs)}$ lies in row labeled as *(B)* in Tab. I, obtained from IST approach [and in row *(D)* for HG2 beam]. It is interesting to note, that, actually, the condition of stationary beam propagation cannot take place neither in the case of HG1 (12) nor HG2 (13) excitation. The HG1 beam splits into two solitons, which propagate apart, and so the distance between these solitons increases with propagation (thus the existence of first order "Gaussian soliton" is again an artifact of variational approach) [see Fig. 2]. The HG2 beam excites in Kerr medium a breather soliton solution, which changes periodically its shape during propagation [see Fig. 3]. The period of self maintaining decreases with increase of the difference $\eta_2 - \eta_1$ [27] [i. e. with increase

of incident amplitude A_0, cf. Fig 1(b)], and, as it is shown in Ref. [29], this is also the case for variational approximation to HG2 beam propagation. For the amplitude corresponding to second–order "Gaussian soliton" excitation the period of oscillation takes non–zero value, but their amplitude is equal to zero (as it is also the case for the fundamental "Gaussian soliton" excitation [15]). Nevertheless, even in this special case, the total field parameters (amplitude and width) can be approximated very accurately by variational solution (see Fig. 10).

IV. COMPARISON OF VARIATIONAL AND NUMERICAL RESULTS

The correspondence between the second–order soliton solution of the NSE and the variational solution with higher–order Hermite–Gaussian ansatz functions can be made vivid by comparison of the results obtained from numerical solution of ODE model (18) with numerical solution of NSE. The NSE is integrated in a finite transverse domain $[-X_0, X_0]$ using the split–step FFT scheme [28] with a mesh $\delta x \approx 0.06$ and $\delta\zeta \approx 0.01$. Numerical accuracy was checked by repeating the simulations for different grid sizes.

In Fig. 5 we compare the presented variational approximation to beam propagation, as obtained from numerical solution of ODE model, with an exact, numerical solution of NSE for HG1 (12) [Figs. 5(a)–(c)] and HG2 (13) [Figs. 5(d)–(f)] incident profiles. The transverse cross–sections of the field are shown at $\zeta = 5z_F$ and $\zeta = 10z_F$ (solid lines), with reference to the incident beam profile at $\zeta = 0$ (dashed line). For the incident beam amplitude below the solitons excitation threshold within the IST approach [compare Tab. I, rows labeled as *(A)*], an excellent agreement between both methods is shown in Fig. 5(a) and Fig. 5(d). The incident beam undergoes nonlinear diffraction and preserves *exactly* its (Hermite–Gaussian of the first– or the second order) form.

For the incident beam amplitude $A_0^{(n)}$ equal to the threshold value for solitons generation, as predicted by IST [see Tab. I, rows *(B)*], small differences between both approaches are illustrated in Fig. 5(b) and Fig. 5(e) for HG1 and HG2 beams, respectively. With an in-

creasing incident beam amplitude $A_0^{(n)}$, variational approximation decreases its quantitative accuracy. Fig. 5(c) and Fig. 5(f) illustrate this fact for the incident beam amplitude which value is taken from rows labeled as *(B)* in Tab. I. In this case only angles of propagation of soliton beams can be estimated accurately from variational approach.

The evolution of the peak amplitudes $|U^{(2)}(x_{max},\zeta)|$ and the locations $\pm x_{max}$ of the peak amplitudes in the plane (x,ζ) are shown in Fig. 6(a) and Fig. 6(b), respectively, for the initial HG2 profile. The values of incident beam amplitudes $A_0^{(2)}$ are those considered in Fig. 5(d)-(f). For incident beam amplitudes below and at the threshold for soliton pair excitation results of variational approach coincide with exact numerical calculations. For the largest incident amplitude $A_0^{(2)}$ displayed in Fig. 6, two solitons with the same amplitudes propagate apart from the ζ-axis. As it is mentioned above, the variational approach predicts in this case the nonlinear diffraction of a beam excited by HG2 incident beam, thus its amplitude decreases, as it is shown in Fig. 6(c). However, the variational method predicts reasonably well an actual propagation angle of the peak amplitude [see Fig. 5(e)]. Similar quantitative and qualitative agreement between variational and numerical calculations has been found for the case of HG1 beam propagation, as it is shown in Fig. 7. In order to compare more systematically the results of direct, numerical solution of NSE with numerical solution of ODE model, we traced the evolution of the peak amplitudes $|U(x_{max},\zeta)|$ and the locations $\pm x_{max}$ of the peak amplitudes in the plane (x,ζ) for different incident beam's amplitudes $A_0^{(n)}$ in both methods. The results obtained at the plane $\zeta = 10z_F = \zeta_0$ are shown in Figs. 8(a) and 8(b) for the case of HG1 and HG2 beam propagation, respectively. For incident amplitudes below the soliton excitation thresholds, predictions of both methods coincides. For higher values of incident amplitudes the discrepancy in values $|U(x_{max},\zeta)|$ is clearly seen (as the result of excitation of soliton pair) but the actuall value of propagation angle is preserved very well within the variational approach to nonlinear beam propagation.

For the incident beam amplitudes above the bound solution formation level $A_0^{(s)}$ no quantitative agreement has been found between predictions of both methods for the initial

HG2 profile. The propagation of the on-axis amplitudes of beams is shown in Fig 9. A very good agreement between both methods is observed for the threshold incident amplitude $A_0^{(thr)}$ (case "A"). For the incident beam amplitude above the bound solution formation level $A_0^{(b)}$ ($A_0^{(2)}$ is taken from the row *(C)* in Tab. I – case "B") variational method predicts periodical pulsation of beam amplitude and width, but with different amplitude and spatial period of oscillations than the actual breather soliton. The case "C" displayed in Fig. 9 corresponds to the case of second-order "Gaussian soliton" propagation, discussed in the previous Section. Thus the ODE model, Eqs. (18), does not allow any changes in the values of beam's width and amplitude, as $P^{(2)}\left(A^{(2)}(0), v(0)\right) = 0$, and so the on-axis amplitude remains constant during propagation.

In Figures 10(a) and 10(b) it is shown, that in the case of second-order "Gaussian soliton" propagation there exist the transverse cross-sections of the beam profiles where, alternatively, the field magnitude of the soliton or the propagation direction of the gravity points of the side lobes preserve the actual values. In other words, the maximal amplitudes are equal at the expense of smearing out the side lobes [see Fig. 10(a)], or the beam widths in both approaches are similar but amplitudes are different. Note, that in this case four discrete eigenvalues occur in the spectrum of the IST [as $A_0^{(gs)}$ lies in row *(D)* in Tab. II, see also Fig. 1(b)].

The variational method is an approximate one and so it can only be as good as the choice of trial function permits. The results obtained from the approximate variational analysis can be misleading as a consequence of the incompleteness of a trial function. Thus a numerical test to validate the variational solutions was necessary. In the case presented in this paper the trial function ansatz [given by Eqs. (16) or (17)] proved to be appropriate for the incident beam amplitudes below the bound solution formation threshold [i. e. for amplitudes displayed in rows *(A)* and *(B)* in Tab. I]. Above this threshold only in the case of symmetric HG2 profile (Figs. 9 and 10) some qualitatively correct assessments can also be made, although the trial function ansatz should be modified to obtain better approximation of the actual beam propagation.

V. CONCLUSION

We have investigated nonlinear propagation of Hermite–Gaussian beams of the first– and second–order in Kerr medium. The initial value problem for the propagation has been solved numerically by use of IST. Considered as the initial condition to NSE, higher–order Hermite–Gaussian function excites an even number of solitons in Kerr medium. These solitons can either propagate in a bisymmetric form (two separated fundamental soliton solutions) from the propagation axis or – in the case of initial HG2 profile – these solitons can form a bound solution in dependence on the incident beam amplitude. By using a variational formulation, we have shown, that the propagation of bisymmetric spatial solitons can be reasonably well modelled by the propagation of higher–order Hermite–Gaussian beam with variationally modified parameters.

APPENDIX A

The effect of an initial electric field profile $U_0^{(n)}(x)$ on the excited soliton parameters ξ_i, η_i ($i = 1, 2, ..., N$, where N is the number of solitons) is given by the solution of the Zakharov-Shabat scattering problem [1,3]

$$\frac{d\varphi_1}{dx} = -i\lambda_i\varphi_1 + i\, U_0^{(n)}(x)\varphi_2 \,, \tag{A1a}$$

$$\frac{d\varphi_2}{dx} = i\lambda_i\varphi_2 + i\, U_0^{(n)*}(x)\varphi_1 \,, \tag{A1b}$$

where $\lambda_i = \xi_i + i\eta_i$ is the complex eigenvalue. The eigenfunctions φ_1 and φ_2, which correspond to soliton solution to NSE, should satisfy certain boundary conditions [see Eqs. (A2) and (A3)]. This eigenvalue problem is overdetermined [30] and there exists no solution for arbitrary value of λ. By introducing the new variable $\varphi_3 = \lambda_i$ one enlarges the set of Eqs. (A1) by adding the new differential equation [30]

$$\frac{d\varphi_3}{dx} = 0 \,. \tag{A1c}$$

The two-point initial conditions, defined at $x = -X_0$ as

$$\begin{pmatrix} \varphi_1(x) \\ \varphi_2(x) \\ \varphi_3(x) \end{pmatrix} = \begin{pmatrix} 1 \\ 0 \\ \lambda^{(\mathrm{guess})} \end{pmatrix} \exp\left(-i\varphi_3 x\right) , \tag{A2}$$

and at $x = X_0$ as

$$\begin{pmatrix} \varphi_1(x) \\ \varphi_2(x) \\ \varphi_3(x) \end{pmatrix} = \begin{pmatrix} 0 \\ b(\varphi_3)\exp\left(i\varphi_3 x\right) \\ \lambda^{(\mathrm{guess})} \end{pmatrix} , \tag{A3}$$

where $|X_0|$ is large enough to cover all nonnegligible values of $U_0^{(n)}(x)$, and $\lambda^{(guess)}$ is the "guess" initial value of λ, lead, after numerical integration, to the soliton parameters ξ_i, η_i. In this way the solution of the eigenvalue problem (A1), with boundary conditions given by Eqs. (A2a–b) and (A3a–b), has been reduced to the standard two-point boundary value problem (more details about this method can be found in Ref. [30]).

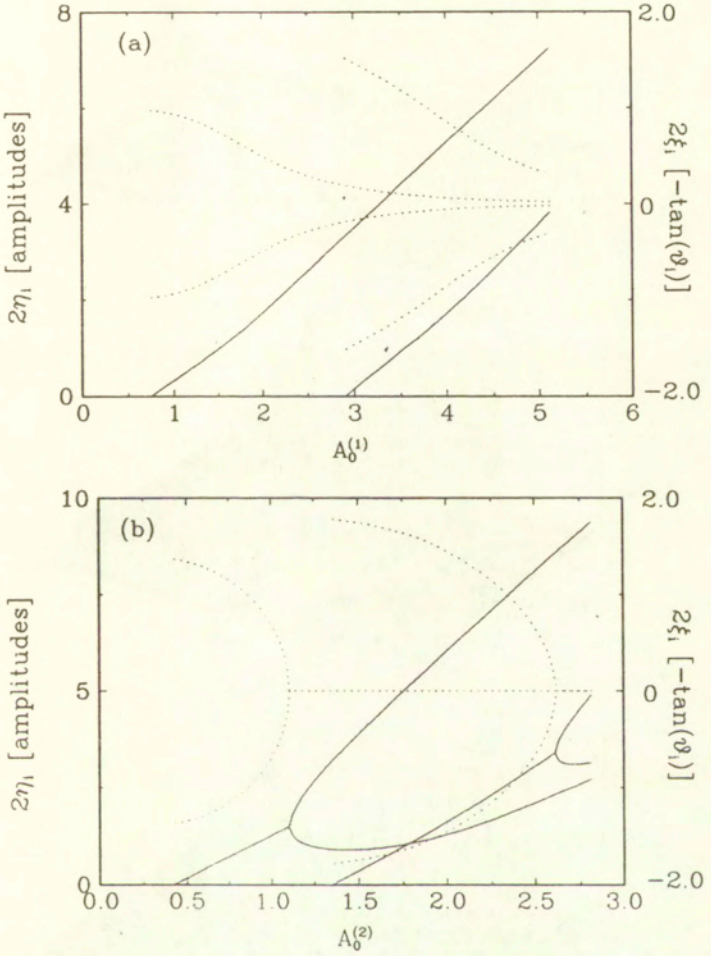

FIG. 1. Soliton parameters excited by the higher–order Hermite–Gaussian beam: (a) – Eq. (12); (b) – Eq. (13). The imaginary parts (solid curves – the left–hand–side axis), and real parts (dotted curves – the right–hand–side axis) of eigenvalues λ_i, $i = 1...4$ (corresponding to the amplitudes and the angles of propagation: $\vartheta_i = -\arctan 2\xi_i$, of solitons, respectively), are plotted as a function of the incident beam amplitude $A_0^{(n)}$.

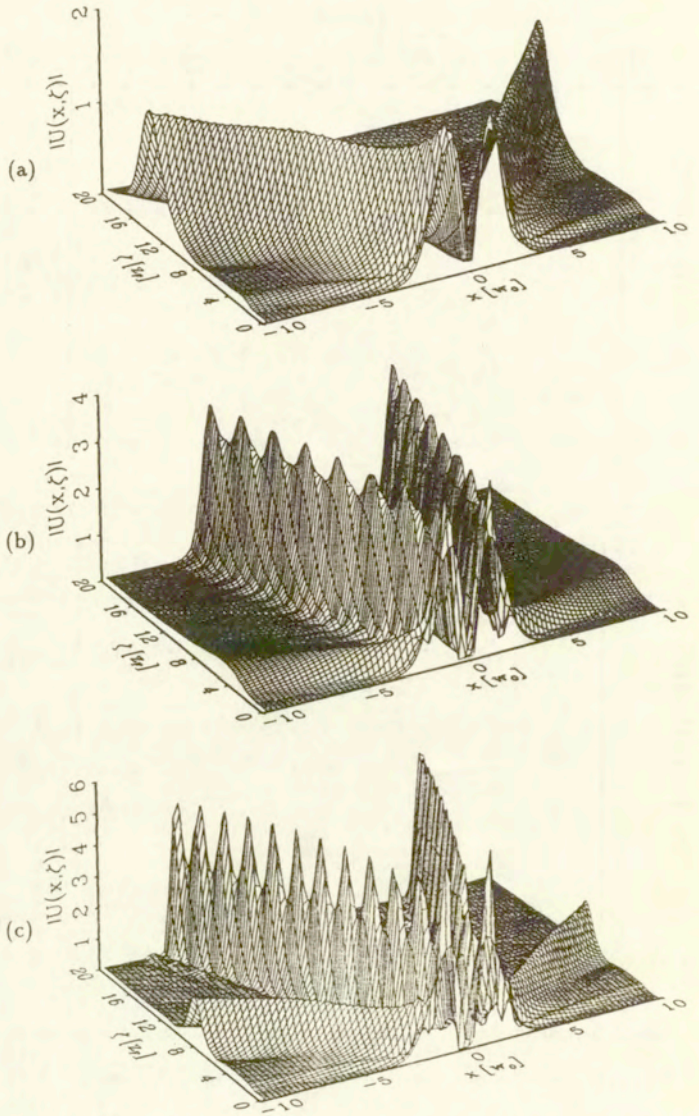

FIG. 2. Evolution of the initial HG1 profile (12) in Kerr medium for various the incident beam amplitudes: (a) $A_0 \approx 1.73$, (b) $A_0 \approx 2.89$, (c) $A_0 \approx 3.91$.

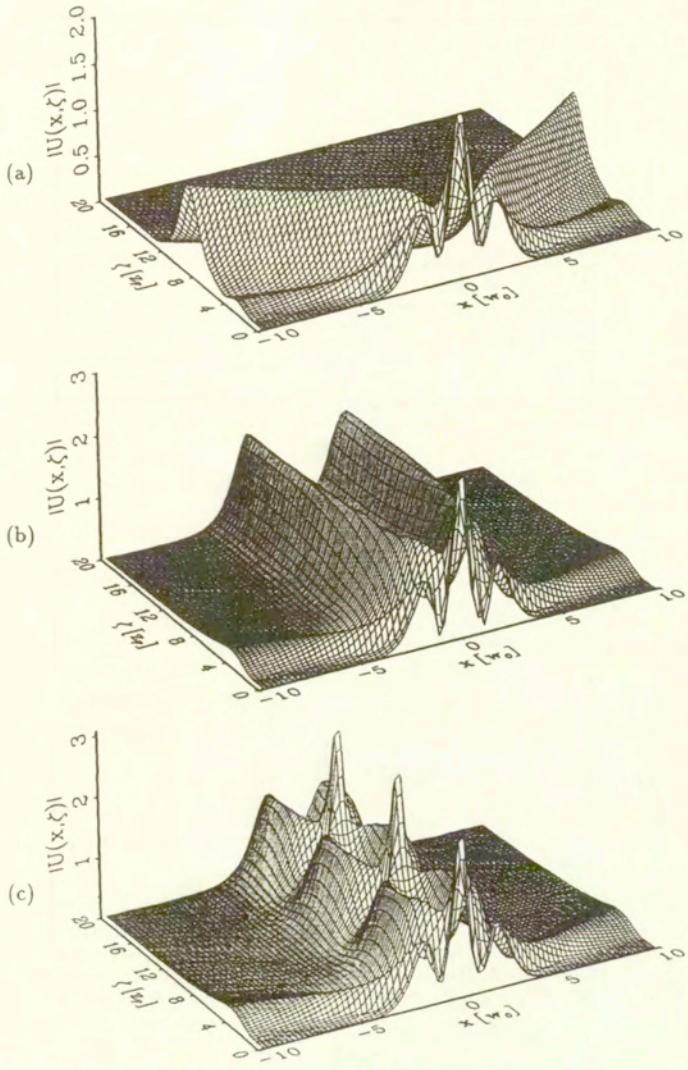

FIG. 3. The same as Fig. (2) but for incident HG2 profile (13). The incident beam amplitudes are: (a) $A_0 \approx 0.83$, (b) $A_0 \approx 1.11$, (c) $A_0 \approx 1.12$.

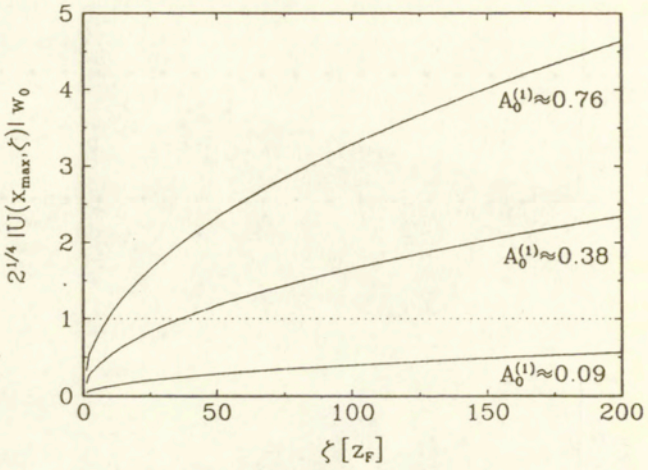

(a)

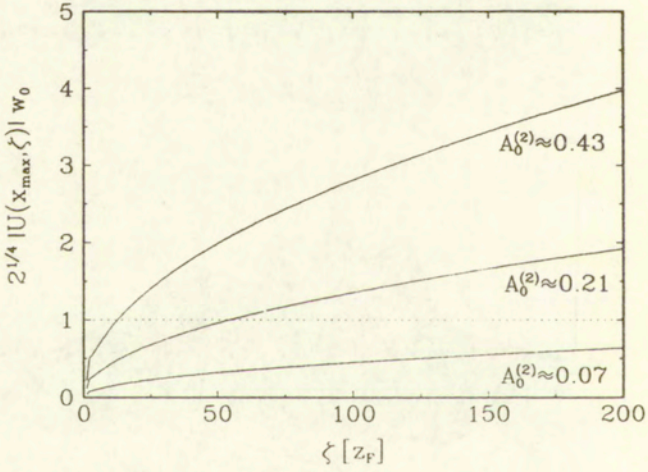

(b)

FIG. 4. Evaluation of the left–hand–side of Eq. (9) for various incident amplitudes of: (a) – HG1 beams, (b) – HG2 beams.

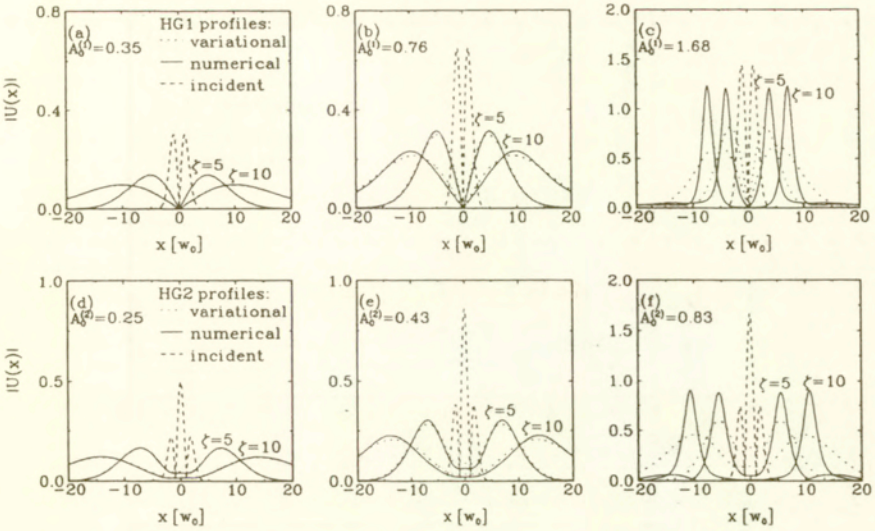

FIG. 5. Comparison of magnitude profiles of solutions of NSE at $\zeta = 5z_F$ and at $\zeta = 10z_F$ as obtained from direct numerical integration of NSE (solid curves) and variational approach (dotted curves). (a)–(c) - propagation of HG1 beams [Eq. (16)]; (d)–(f) - propagation of HG2 beams [Eq. (17)]. The incident HG profiles at $\zeta = 0$ (dashed curves) are shown for comparison. The incident beam amplitudes are: (a) $A_0^{(1)} = 0.35$, (b) $A_0^{(1)} = 0.76 = A_0^{(thr)}$, (c) $A_0^{(1)} = 1.68$, (d) $A_0^{(2)} = 0.25$, (e) $A_0^{(2)} = 0.43 = A_0^{(thr)}$, (f) $A_0^{(2)} = 0.83$.

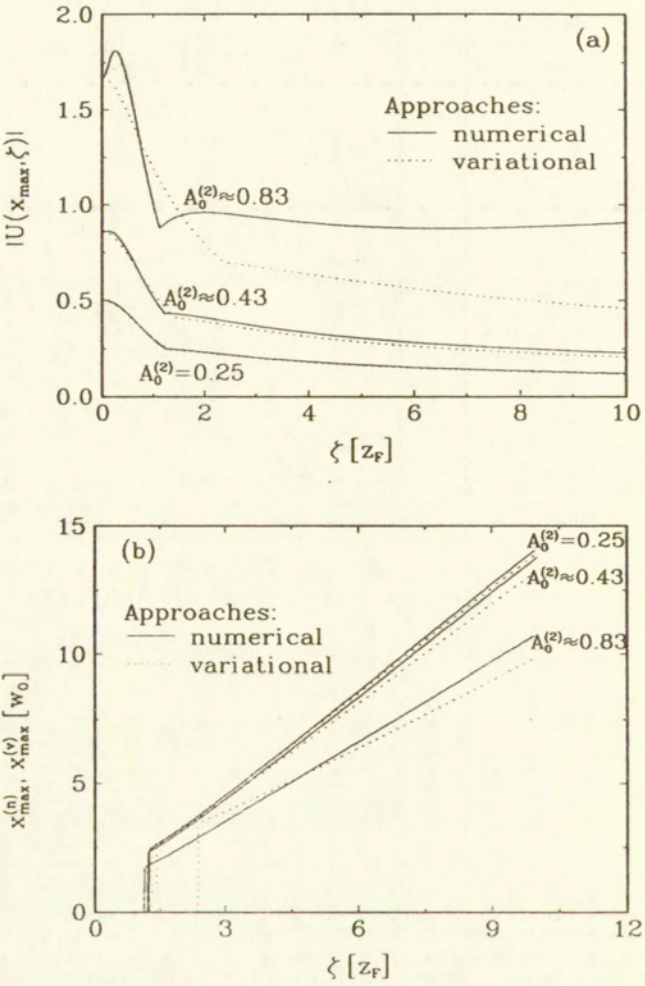

FIG. 6. (a) Peak amplitudes of the beams in variational $|U^{(2)}(x_{max}^{(v)},\zeta)|$ and numerical $|U(x_{max}^{(n)},\zeta)|$ approaches vs propagation distance ζ for the incident HG2 profile (13). (b) Location of the peak amplitudes $x_{max}^{(v)}$ and $x_{max}^{(n)}$ of the beams on a (x,ζ) plane. Solid curves – numerical calculations, dotted curves – variational approximation. The incident beam amplitudes $A_0^{(2)}$ are displayed on a plot.

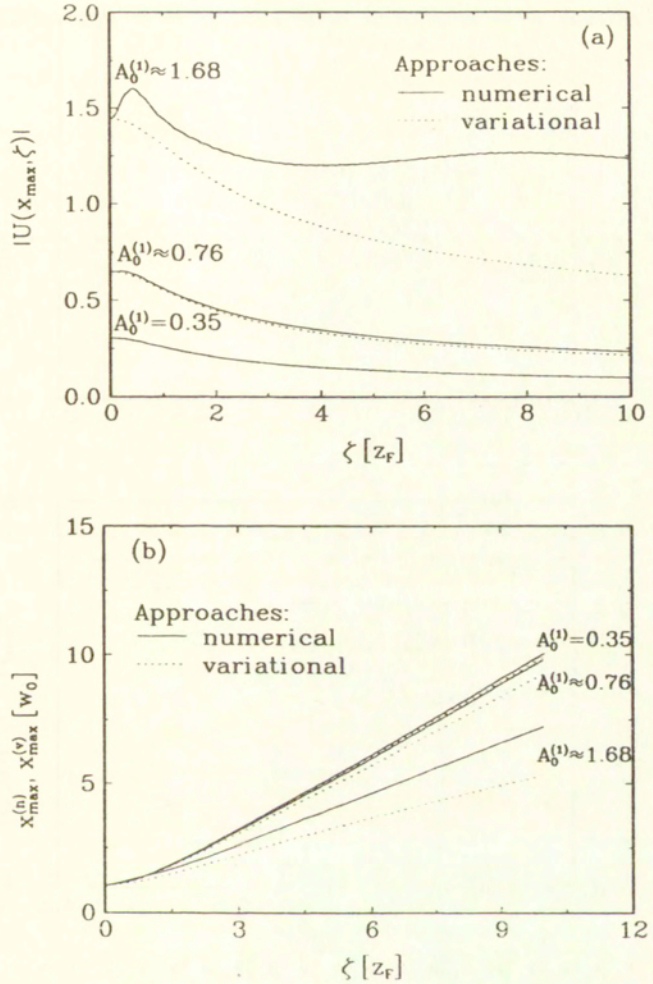

FIG. 7. The same as Fig. (6) but for the incident HG1 profile (12).

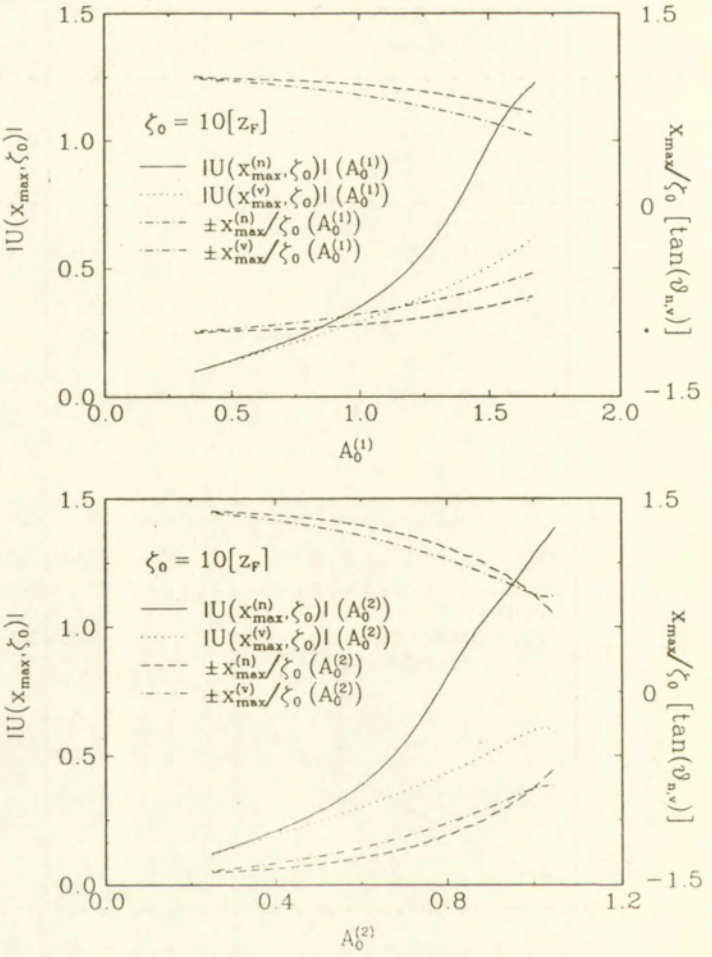

FIG. 8. Left-hand-side axis: Peak amplitudes of the beams $|U^{(n)}(x_{max},\zeta_0)|$ in numerical (solid line) and variational (dotted line) approaches evaluated at $\zeta_0 = 10z_F$ vs the amplitude of the incident beam $A_0^{(n)}$. Right-hand-side axis: The angles of propagation $\tan\vartheta_{(n,v)} = x_{max}^{(n,v)}/\zeta_0$ vs $A_0^{(n)}$ in numerical (dashed line) and variational (dashed-dotted line) approaches. (a) - HG1 beam propagation, (b) - HG2 beam propagation.

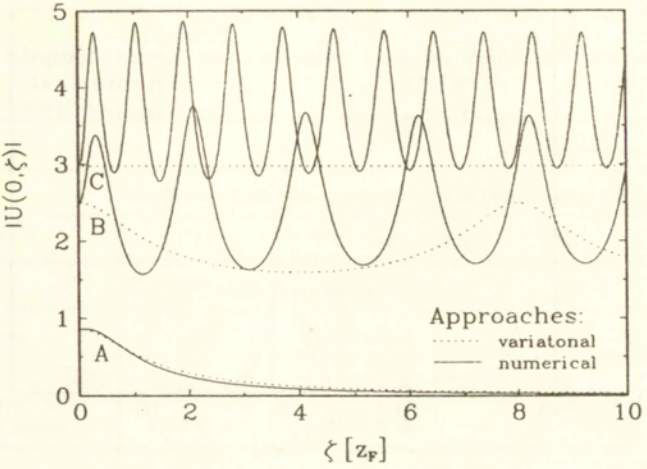

FIG. 9. Beam amplitudes $|U^{(2)}(x,\zeta)|$ at the center of the beams ($x = 0$) vs ζ in numerical (solid curves) and variational (dotted curves) approaches. The incident beam amplitudes are: A – $A_0^{(2)} \approx 0.43$; B – $A_0^{(2)} = 1.25$; C – $A_0^{(2)} \approx 1.48$.

TABLE II. The reduced Lagrangians, Hamiltonians, and the functions $P^{(n)}(A,v)$ and $Q^{(n)}(A,v)$, as obtained from variational analysis of Hermite–Gaussians propagation in Kerr medium. $Re[a]$ and $Im[a]$ denote the real and imaginary part of the complex quantity a, respectively.

	0^{th} order Hermite-Gaussians
Lagrangian	$\frac{-\sqrt{2\pi}}{(v^2+v^{*2})^{3/2}}\left[2Re[v^2]Im[A^*\dot{A}]+\lvert A\rvert^2\left(Im[v^*\dot{v}^*]+\frac{1}{2}\right)-\frac{\lvert A\rvert^4}{\sqrt{2}\lvert v\rvert^2}Re[v^2]\right]$
Hamiltonian	$\sqrt{\frac{\pi}{2}}\frac{\lvert A\rvert^2}{(v^2+v^{*2})^{3/2}}\left[1-\frac{\sqrt{2}\lvert A\rvert^2}{\lvert v\rvert^2}Re[v^2]\right]$
$P^{(0)}(A,v)$	$\frac{i}{2v}-\frac{i}{8}A_0^2\left(1+\frac{v^2}{v^{*2}}\right)^{3/2}$
$Q^{(0)}(A,v)$	$\frac{i}{2}A_0^2\sqrt{\frac{1}{v^2}+\frac{1}{v^{*2}}}\left(1-\frac{v^2}{4v^{*2}}\right)A$
	1^{st} order Hermite-Gaussians
Lagrangian	$\frac{-2\sqrt{2\pi}}{(v^2+v^{*2})^{5/2}}\left[2Re[v^2]Im[A^*\dot{A}]+3\lvert A\rvert^2\left(Im[v^*\dot{v}^*]+\frac{1}{2}\right)-\frac{3}{4\sqrt{2}}\frac{\lvert A\rvert^4}{\lvert v\rvert^2}\right]$
Hamiltonian	$\sqrt{\frac{\pi}{2}}\frac{6\lvert A\rvert^2}{(v^{*2}+v^2)^{5/2}}\left[1-\frac{\lvert A\rvert^2}{2\sqrt{2}\lvert v\rvert^2}\right]$
$P^{(1)}(A,v)$	$\frac{i}{2v}-\frac{i}{32}A_0^2\left(1+\frac{v^2}{v^{*2}}\right)^{3/2}$
$Q^{(1)}(A,v)$	$\frac{3i}{4\sqrt{2}}A_0^2\sqrt{\frac{1}{v^2}+\frac{1}{v^{*2}}}\left(1-\frac{v^2}{4v^{*2}}\right)A$
	2^{nd} order Hermite-Gaussians
Lagrangian	$\frac{-12\sqrt{2\pi}}{(v^2+v^{*2})^{9/2}}\left[2\left(\lvert v\rvert^2+Re[v^4]\right)Im[A^*\dot{A}]+5\lvert A\rvert^2Im[v^{*3}\dot{v}^*]\right.$ $\left.+\lvert A\rvert^2\left(\frac{35}{8}\lvert v\rvert^2Im[v\dot{v}^*]+5Re[v^2]\right)-\frac{\lvert A\rvert^4}{\sqrt{2}\lvert v\rvert^{10}}\left(Re[v^8]+\lvert v\rvert^4Re[v^4]+\frac{35}{8}\lvert v\rvert^8\right)\right]$
Hamiltonian	$\frac{12\sqrt{\pi}\lvert A\rvert^2}{(v^{*2}+v^2)^{9/2}}\left[5\sqrt{2}Re[v^2]-\frac{\lvert A\rvert^2}{\lvert v\rvert^{10}}\left(Re[v^8]+\lvert v\rvert^4Re[v^4]+\frac{35}{8}\lvert v\rvert^8\right)\right]$
$P^{(2)}(A,v)$	$\frac{i}{2v}-\frac{i}{8}A_0^2\left(1+\frac{v^2}{v^{*2}}\right)^{3/2}\left[\frac{43}{80}+\frac{7}{20}\frac{v^2}{v^{*2}}+\frac{5}{20}\frac{v^4}{v^{*4}}-\frac{1}{20}\frac{v^{*2}}{v^2}-\frac{5}{20}\frac{v^{*4}}{v^4}-\frac{4}{20}\frac{v^{*6}}{v^6}\right]$
$Q^{(2)}(A,v)$	$iA_0^2\sqrt{\frac{1}{v^2}+\frac{1}{v^{*2}}}\left[\frac{9}{4}-\frac{27}{64}\frac{v^2}{v^{*2}}+\frac{9}{16}\frac{v^{*2}}{v^2}-\frac{3}{16}\frac{v^4}{v^{*4}}+\frac{1}{2}\frac{v^{*4}}{v^4}-\frac{5}{16}\frac{v^6}{v^{*6}}\right]A$

REFERENCES

[1] V. E. Zakharov, A. B. Shabat, "Exact theory of two–dimensional self–focusing and one–dimensional self–modulation of waves in nonlinear media," (in Russian) Zh. Exp. Teor. Fiz. **61**, pp. 118–134 (1971).

[2] A. Hasegava, F. Tappert, "Transmission of stationary nonlinear optical pulses in dispersive dielectric fibers. I. Anomalous disspersion," Appl. Phys. Lett. **23**, pp. 142–144 (1973).

[3] J. Satsuma, N. Yajima, "Initial value problems of one–dimensional self–modulation of nonlinear waves in dispersive media," Suppl. Prog. Theor. Phys., No. **55**, pp. 284–306 (1974).

[4] L. F. Mollenauer, R. H. Stolen, J. P. Gordon, "Experimental observation of picosecond pulse narrowing and solitons in optical fibers," Phys. Rev. Lett. **45**, pp. 1095–1098 (1980).

[5] L. F. Mollenauer, K. Smith, "Demonstration of soliton transmission over more than 4000 km in fiber with loss periodically compensated by Raman gain," Opt. Lett. **13**, pp. 675–677 (1988).

[6] M. Nakazawa, H. Kubota, K. Kurokawa, E. Yamada, "Femtosecond optical soliton optical soliton transmission over long distances using adiabatic trapping and soliton standarization," J. Opt. Soc. Am. B 8, pp. 1811–1817 (1991).

[7] S. Maneuf, R. Desailly, C. Froehly, "Stable self–trapping of laser beams: observation in nonlinear planar waveguide," Opt. Commun. 65, pp. 193–198 (1988).

[8] J. S. Aitchison, A. M. Weiner, Y. Silberberg, M. K. Oliver, J. L. Jackel, D. E. Leaird, E. M. Vogel, P. W. E. Smith, "Observation of spatial optical solitons in nonlinear glass waveguide," Opt. Lett. **15**, pp. 471–473 (1990).

[9] S. Barthelemy, S. Maneuf, C. Froehly, "Propagation soliton et auto–confinement de

faisceaux laser par nonlinearite' optique de Kerr," Opt. Commun. **55**, pp. 201–206 (1985).

[10] G. Khitrova, H. M. Gibbs, Y. Kawamura, H. Iwamura, T. Ikegami, J. E. Sipe, L. Ming, "Spatial solitons in a self–focusing semiconductor gain medium," Phys. Rev. Lett. **70**, pp. 920–923 (1993).

[11] S. Wabnitz, E. M. Wright, C. T. Seaton, G. I. Stegeman, "Instabilities and all–optical phase–controlled switching in a nonlinear directional coherent coupler," Appl. Phys. Lett. **49**, pp. 838–840 (1986).

[12] A. B. Aceves, J. V. Moloney, A. C. Newell, "Theory of light–beam propagation at nonlinear interfaces. I. Equivalent–particle theory for a single interface", Phys. Rev. A. **39**, pp. 1809–1827 (1989).

[13] T. Ueda, W. L. Kath, "Dynamics of coupled solitons in nonlinear optical fibers", Phys. Rev. A **42**, pp. 563–571 (1990).

[14] C. Pare, M. Florjanczyk, "Approximate model of soliton dynamics in all–optical couplers", Phys. Rev. A **41**, 6287–6295 (1990).

[15] D. Anderson, "Variational approach to nonlinear pulse propagation in optical fibers", Phys. Rev. A **27**, pp. 3135–3145 (1983).

[16] M. Desaix, D. Anderson, M. Lisak, "Variational approach to collapse of optical pulses", J. Opt. Soc. Am. B **8**, pp. 2082–2086 (1991).

[17] J. P. Gordon, "Interaction forces among solitons in optical fibers", Opt. Lett. **8**, pp. 596–598 (1983).

[18] W. Nasalski, "Linear formulation of nonlinear propagation of optical beams and pulses", Optica Applicata **24**, no. 4 (1994), in press

[19] D. Burak, W. Nasalski, "Spatial solitons excited by the second–order Hermite–Gaussian

beams", Optica Applicata, **24**, no. 4 (1994), in press.

[20] J. A. Arnaud, Beams and Fiber Optics (Academic Press, New York, 1976).

[21] A. E. Siegman, "Hermite–Gaussian functions of complex argument as optical–beam eigenfunctions", J. Opt. Soc. Am., **63**, pp. 1903–1904 (1973).

[22] W. Nasalski, "Nonspecular bistability versus diffraction at nonlinear hybrid interfaces," Opt. Commun. **77**, pp. 443–450 (1990); "Ray analysis of Gaussian beam nonspecular scattering," Opt. Commun. **92**, pp. 307–314 (1992).

[23] Y. M. M.Antar and W. M. Boerner, "Generation of complex Gaussian beam modes in beam interaction with planar dielectric interface," I.E.E.E. Trans. on Antennas and Propagation, AP–**22**, pp. 837–839 (1974).

[24] T. Takenaka, M. Yokota and O. Fukumitsu, "Propagation of light beams beyond the paraxial approximation," J. Opt. Soc. Am. A **2**, pp. 826–829 (1985).

[25] W.Nasalski, "Complex ray tracing of the soliton propagation", to be published.

[26] D. Burak, W. Nasalski, "Gaussian beam to spatial soliton formation in Kerr medium", Appl. Opt., **33**, pp. 6393–6401 (1994).

[27] H. A. Haus, M. N. Islam, "Theory of the soliton laser", IEEE J. Quantum Electron. **21**, pp. 1172–1188 (1985).

[28] G. P. Agrawal, Nonlinear Fiber Optics, (Academic Press, New York, 1989), pp. 44–48.

[29] D. Burak, "Steering of bright spatial solitons using second–order Hermite–Gaussian beams", to be published.

[30] H. Press, B. P. Flannery, S. A. Teukolsky, W. T. Vetterling, Numerical Recipes, 2 nd ed. (Cambridge Univ. Press, Cambridge, 1992), Chap. 17, p. 745.